Front. Struct. Civ. Eng. 2023, 17(5): 686–703
https://doi.org/10.1007/s11709-023-0937-2

RESEARCH ARTICLE

Performance evaluation of low-rise infilled reinforced concrete frames designed by considering local effects on column shear demand

Jarun SRECHAI[a], Wongsa WARARUKSAJJA[b*], Sutat LEELATAVIWAT[c], Suchart LIMKATANYU[d]

[a] *Department of Civil Engineering, Faculty of Engineering, Burapha University, Chon Buri 20131, Thailand*
[b] *Department of Civil Engineering, Faculty of Engineering, Rajamangala University of Technology Thanyaburi, Pathum Thani 12110, Thailand*
[c] *Department of Civil Engineering, Faculty of Engineering, King Mongkut's University of Technology Thonburi, Bangkok 10140, Thailand*
[d] *Department of Civil Engineering, Faculty of Engineering, Prince of Songkla University, Songkla 90110, Thailand*
[*] *Corresponding author. E-mail: wongsa.w@en.rmutt.ac.th*

ABSTRACT The interactions between reinforced concrete (RC) frames and infill walls play an important role in the seismic response of frames, particularly for low-rise frames. Infill walls can increase the overall lateral strength and stiffness of the frame owing to their high strength and stiffness. However, local wall-frame interactions can also lead to increased shear demand in the columns owing to the compressive diagonal strut force from the infill wall, which can result in failure or in serious situations, collapse. In this study, the effectiveness of a design strategy to consider the complex infill wall interaction was investigated. The approach was used to design example RC frames with infill walls in locations with different seismicity levels in Thailand. The performance of these frames was assessed using nonlinear static, and dynamic analyses. The performance of the frames and the failure modes were compared with those of frames designed without considering the infill wall or the local interactions. It was found that even though the overall responses of the buildings designed with and without consideration of the local interaction of the infill walls were similar in terms the overall lateral strength, the failure modes were different. The proposed method can eliminate the column shear failure from the building. Finally, the merits and limitations of this approach are discussed and summarized.

KEYWORDS reinforced concrete frames, infill wall, seismic design method, shear failure, wall-frame interaction

1 Introduction

Reinforced concrete (RC) frames with masonry infill walls are commonly used as structural systems in seismically active areas within many countries, especially for low- to medium-rise buildings. It is well understood that the seismic performance of building structures is significantly influenced by the presence of infill walls [1,2]. Research has indicated that infill walls can have both beneficial and adverse effects on the seismic responses of structures [3–9]. Infill walls can augment the overall lateral strength and stiffness of the frame, resulting in a higher seismic resistance. In contrast, an increase in the stiffness can also cause a higher seismic demand [10]. At the global response level, the presence of infill walls can lead to building irregularities both in plan and elevation, such as soft-story and torsional irregularities [6]. More critically, the local interaction between the infill wall and the frame can increase the internal forces in the surrounding members. This can result in an undesirable failure mode, such as shear failure of the column or, in more serious cases, the loss of the gravity load-carrying capacity, leading to collapse, even at low drift levels [11]. Therefore, if the failure of the surrounding members can be prevented, the frame can gain significant seismic resistance by harnessing the

Article history: Received Feb 26, 2022; Accepted Dec 3, 2022

additional strength and stiffness of the infill walls.

Numerous experimental and analytical studies [12–25] have been conducted to investigate the effect of infill walls on the structural response. Based on these studies, the behavior of infilled RC frames depends strongly on both the frame and infill wall failure characteristics. For the frame, failure is dominated by column shear failure or column flexural hinges. According to previous studies, several failure modes of infill walls have been identified, such as diagonal shear sliding, sliding along the bed joint, and corner crushing. Nevertheless, Huang and Burton [26] indicated that only two failure patterns are observed for infill walls. These are diagonal shear sliding and combined sliding-crushing. These failure modes can be followed by flexural or shear failure of the surrounding columns depending on the relative strength of the infill walls compared with that of the surrounding columns. As a result of the high shear demand produced by the wall-frame interaction, column shear failure can occur even though the frame was designed to be ductile. Therefore, the wall-frame interaction on the surrounding frames cannot be overlooked even for ductile frames and even more so for frames with a low level of ductility. As reported by Milanesi et al. [22], in some cases, the column shear demand in the frame members could be almost four times larger than that in the bare frame.

For analysis and design purposes, the complex interactions between the frame and the infill wall are considered using different approaches [27]. Several modeling techniques to capture the stiffness and interactions of infill walls have been studied. One of the earliest attempts to capture the infill wall presence was to model the infill wall as an equivalent diagonal strut with the cross-section calibrated to provide equivalent strength and stiffness of the wall [3]. This approach can represent the overall stiffness and strength of the wall but is not effective in capturing the local interactions between the frame and the infill wall. Improvements in the modeling technique include the use of multiple struts to represent the infill wall [11,28–31]. The placement of the struts and their properties were properly tuned to provide equivalent strength and stiffness of the wall and to introduce an additional shear force in the surrounding frame members. Recent developments include the use of a data-driven multiple strut model that was developed and calibrated based on a comprehensive experimental database and regression analysis covering different infill types, frame types (ductile and nonductile), and failure modes [32]. More comprehensive micro-modeling based on detailed finite element analysis has also been widely used to investigate the detailed behavior and interactions between the surrounding frame and infill wall [20–22,33]. This type of micro-modeling approach can capture detailed information, including global and local interactions, and interface stress distributions. Although these types of detailed models (multiple struts and detailed finite element methods) can provide comprehensive information on the response of the infilled frames, they are more valuable for research and nonlinear performance evaluation at the final stage. They are not compatible with current design practices. In general, only bare frame models are used during the design stage. Infill walls are generally treated as non-structural elements. These are only included as additional distributed loads and masses. Stiffness and wall-frame interactions are generally ignored. This may have serious consequences, as previously mentioned. The practical and effective consideration for infill walls in design remains an open question.

In terms of design codes, clear guidelines are lacking. In general, the code approaches either allow the infill wall-frame interaction to be considered or require the infill walls to be isolated from the frames, eliminating the complex interaction altogether. Eurocode 8 [34] and ASCE/SEI 41-17 [35] provide broad recommendations for considering the wall-frame interaction in the design process. The surrounding column should be designed to prevent the potential captive column mechanism from being induced by the infill wall. However, clear guidelines for estimating the shear demand and shear capacity of columns have not been provided. Recently, Wararuksajja et al. [19] proposed an effective design strategy to consider infill-frame interactions. This approach was based on the plastic mechanism analysis of the column. In this approach, the infilled frames are analyzed and designed as bare frames in the first step, following conventional design practice. Additional steps were then applied to prevent local failure of the surrounding columns. The columns were checked for increased shear demand at the local level at different response levels, and necessary design measures were applied to counteract the adverse effects of the infill walls. By preventing the failure of the surrounding members, the frame can gain significant seismic resistance owing to the additional strength and stiffness of the infill wall. The advantage of this approach is that no radical changes to common design practices are required. The adverse effects of the infill walls are considered in a systematic manner. If needed, the global effects and irregularity owing to the presence of the infill wall can also be considered by using only the single equivalent strut model and significantly simplifying the modeling process.

The effectiveness of the design method was verified through experiments and analysis, as reported by Wararuksajja et al. [36]. Appropriate design formulas and parameters are recommended. They concluded that using this design method as a supplement to the code-based design approach can effectively prevent column shear failure. However, the verification was only performed on a single-bay and single-story infilled RC frame test specimen without considering the global response of the building. Realistic frame structures were not considered in their study.

The current study aims to evaluate the above design method when applied to realistic frame structures. The main concept of the design approach is briefly reviewed. The approach is then applied to design prototype RC frames with infill walls located in areas with different seismicity levels in Thailand. The performance of these frames is assessed using nonlinear static and dynamic analyses. The performance of the frames, failure modes, and accuracy of the design method are discussed and compared with those of frames designed without considering the infill wall or the local interactions. Based on the performance evaluation, the effectiveness, limitations, and essential improvements of the proposed design approach are discussed.

2 Method

2.1 Design considering local infill-frame interaction

To prevent the local failure of columns due to wall-frame interactions, several different approaches have been recommended by national building codes [27]. The most widely used methods suggested by Eurocode 8 [34] and ASCE/SEI 41-17 [35] are summarized herein. A new design method proposed by Wararuksajja et al. [19] is then briefly reviewed.

Eurocode 8 [34] states that the shear in the column in the critical region should be verified. The contact length of the column and infill strut is considered to be the critical region for the solid infilled frames. The column shear demand in that region is taken as the lesser of (i) the infill wall's horizontal shear strength estimated following the bed joint strength, and (ii) the resulting shear force obtained by assuming plastic hinges are formed at the ends of the contact length. In this method, the contact length is assumed to be equal to the full vertical width of the infill strut. However, the code only provides a broad recommendation for estimating the infill strut width as a fraction of the diagonal length of the infill wall.

A similar criterion with minor modifications was also adopted for ASCE/SEI 41-17 [35]. The code suggests that the shear strength of the column should be greater than the force estimated by one of the following conditions. The first relates to the force due to the horizontal component of the infill strut force applied to the column. The other relates to the shear force obtained by assuming that plastic hinges develop at both ends of the column with a reduced length. The infill strut properties can be determined based on the difference between the envelope curves of the infilled frame and associated bare frame. For a reduced column length, neither a formula nor a specific guidance is suggested. However, this requirement is not essential for a masonry shear strength < 0.138 MPa.

Recently, Wararuksajja et al. [19] proposed a practical design approach to prevent captive column shear failure owing to wall-frame interactions. The flexural strength of the column was first determined using a code-based frame analysis. The column shear demand and shear capacity due to wall-frame interaction were then examined at different response states using plastic mechanism analysis. In this approach, an infill wall is represented by an equivalent compressive strut. The strut axial force capacity (C_i) can be estimated using a chosen method depending on the expected failure modes of the wall [4,12,13,35,37–41]. The force of the damaged infill struts is assumed to be αC_i, where α is a reduction factor that decreases the strut force from the original force. As in the Eurocode 8 and the ASCE/SEI 41-17 standards, two possible outcomes are considered. These include the column-infill mechanism for a frame with relatively strong columns, and the column mechanism for a frame with relatively weak columns (Fig. 1). For the column-infill mechanism, the infill crushing zone continues to expand until plastic hinges form at the column ends (Fig. 1(a)). Column shear (V_a) can be estimated based on the plastic hinges at the ends of the columns and the compressive force from the residual strut, as shown in Eq. (1).

$$V_a = \frac{2M_p}{H_w} + \frac{\alpha C_i \cos\theta (H_w - a)}{H_w}, \tag{1}$$

where a is the dimension of the infill wall crushing zone, H_w is the wall height, θ is the angle of the strut, and M_p is the flexural capacity of the column. In certain cases, M_p can be less than the flexural capacity of the column when M_p is limited by the beam plastic moment framing of the joint.

For the column mechanism, the remaining wall was stronger than the column. The undamaged portion of the infill wall below the crushing zone can restrict the deformation of the column, leading to captive column failure (Fig. 1(b)). In this case, the column shear demand (V_b) can be estimated using Eq. (2).

$$V_b = \frac{2M_p}{a}. \tag{2}$$

The required shear strength of the column (V_u) corresponds to the lower shear force obtained from Eqs. (1) and (2), respectively:

$$V_u = \min(V_a, V_b). \tag{3}$$

The reduction factor is developed using the results of the finite element method analysis of an RC frame with an infill wall, as reported by Wararuksajja et al. [36]. The following equation was proposed for the reduction factor in terms of the gap opening, a:

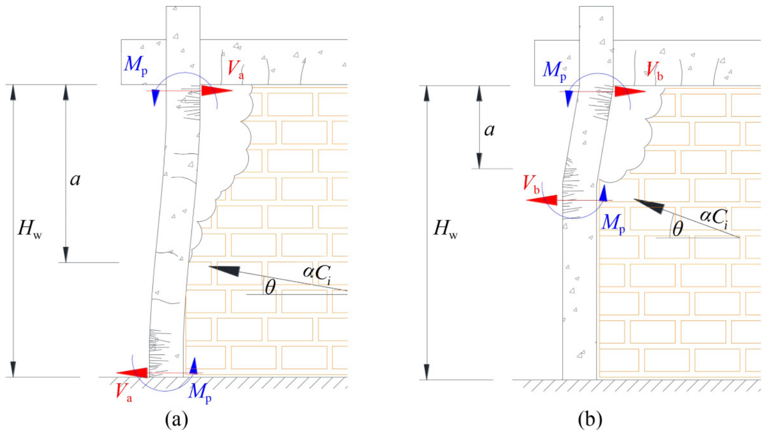

Fig. 1 Failure mechanism: (a) column-infill; (b) column (modified from Ref. [19]). (Reprinted from Bulletin of Earthquake Engineering, 18(14), Wararuksajja W, Srechai J, Leelataviwat S, Seismic design of RC moment-resisting frames with concrete block infill walls considering local infill-frame interactions, 6445–6474, Copyright 2020, with permission from Springer Nature.)

$$\begin{aligned} &\alpha = 1.0, && \text{for} \quad \frac{a}{H_w} < 0.05, \\ &\alpha = 1.05 - 1.1\frac{a}{H_w}, && \text{for} \quad 0.05 \leqslant \frac{a}{H_w} \leqslant 0.60, \\ &\alpha = 0.4, && \text{for} \quad \frac{a}{H_w} > 0.60. \end{aligned} \tag{4}$$

Once the shear demand is established, the shear force in the column can be checked against the column capacity. The shear capacity of the column varies based on the shear span ratio (a/d), which depends strongly on the dimensions of the unrestrained region (a). A strut-and-tie model is best suited for calculating the column shear strength [42,43] for a small gap opening (low shear span ratio). In this case, the column shear strength is dictated by the strength of the diagonal compression strut in the column. The shear strength (V_n) formula proposed by Li and Hwang [44] is recommended by Wararuksajja et al. [36]:

$$V_n = \lambda_s f_c' A_{str} \cos\varphi, \tag{5}$$

where φ is the angle of the compression strut with respect to the horizontal axis, f_c' is the compressive strength (MPa), A_{str} is the cross-sectional area of the compression strut (mm^2), and λ_s is the strut-and-tie numerical index [44] depending on the amount of reinforcement and the compression strut angle.

As the drift increases and the damage in the infill wall expands, resulting in a large gap opening (larger than approximately four times the column depth), the shear strength (V_n) of the column can be estimated using code-based formulas. In the present study, the shear strength formula recommended by ACI 318/318R-14 [45] was used.

The proposed design steps essentially involve calculating the shear demand and shear strength based on the assumed opening length (a). The calculation process is repeated by gradually increasing the opening dimension (a) until it extends to cover a reasonable portion of the column. The details of this method are summarized elsewhere [19,36].

2.2 Study frames and preliminary evaluation

To investigate the effectiveness of the proposed design strategy, a typical low-rise commercial building, commonly found in Thailand, was selected, and its seismic performance was assessed using nonlinear static and dynamic analyses. A four-story masonry infilled RC building with eight and three bays in the longitudinal and transverse directions, respectively, (denoted as x and y, respectively) was selected as a prototype. A typical story was 3 m in height and 4 m in span length. For the base story, column piers 1 m in height were used to connect the foundation and the ground floor, as illustrated in Fig. 2. Masonry infill walls with and without openings were used as partitions for the building. These buildings are assumed to be located in areas with low and high seismicity levels in Thailand. In the low-seismicity area, the design spectral acceleration values at 0.2 (S_s) and 1 s periods (S_1) were 0.434g and 0.122g, respectively. For the high-seismicity area, S_s and S_1 were 1.086g and 0.275g, respectively.

In this study, two design scenarios were examined. In the first scenario, the building was analyzed and designed as if it was only a bare frame, without any consideration for the infill walls, following a conventional design method. For low-seismicity areas, the frame was designed as an intermediate moment-resisting RC frame [45]. For high-seismicity areas, the frame was designed as a special moment-resisting RC frame. The buildings are denoted as building B1 and building B2 for the low- and high-seismicity areas, respectively. The seismic performance of each code-designed building was assessed using nonlinear, static, and dynamic analyses. In the second design scenario, after the flexural design of the columns, additional steps following the design method proposed by

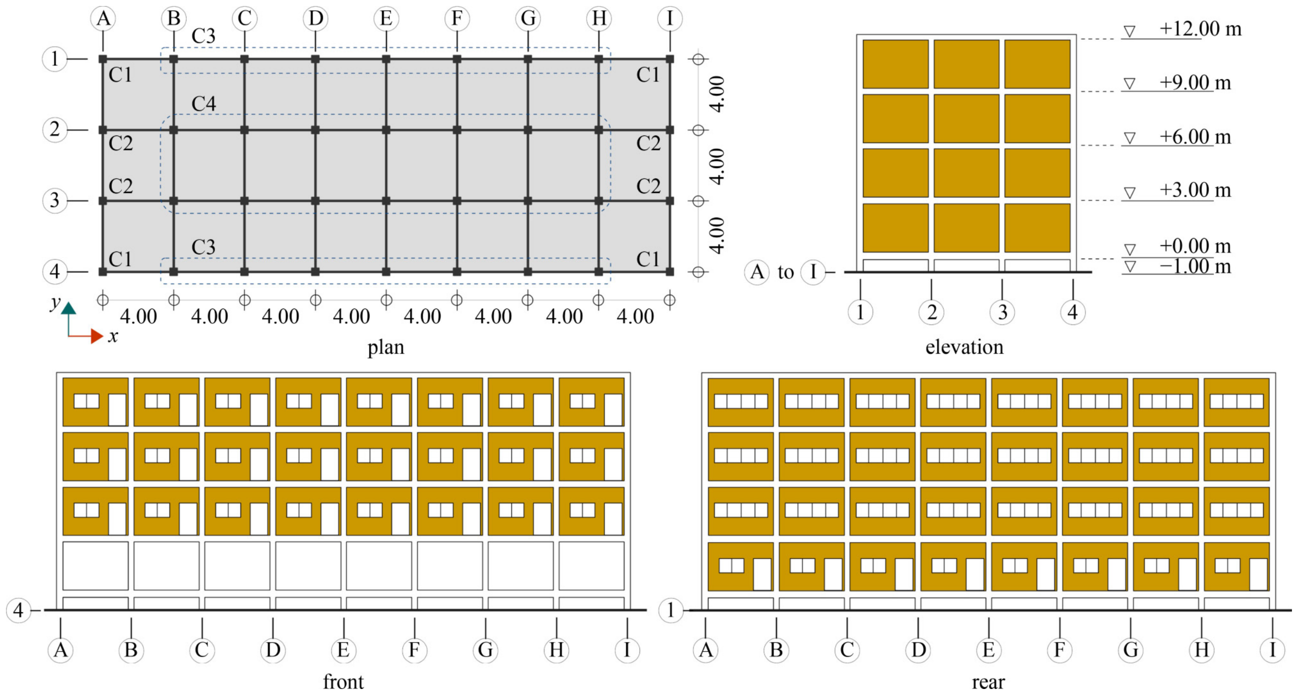

Fig. 2 Masonry infilled RC building used in this study.

Wararuksajja et al. [19] were performed to estimate the appropriate column shear strength. If necessary, the concrete strength, column size, and column shear reinforcement bars were altered to provide a sufficient column shear strength. The compressive strength of the concrete was first increased to increase the column shear strength. If this was insufficient, column size and shear reinforcement alterations were made. It should be noted that this process was applied to the columns for all stories even though the high column shear demands were generally concentrated only in the lower stories. In this study, the nominal yield strengths (f_y) of the longitudinal and transverse reinforcement bars were assumed to be 400 MPa. Concrete with a compressive strength (f'_c) of 21 MPa was used for buildings B1 and B2 and 28 MPa was used for the redesigned building. Masonry infill walls with an average compressive strength of 6.5 MPa were used in both cases.

The cross-sectional dimensions and reinforcement details of the columns and beams of the designed building B1 and building B2 following the conventional design method without considering the infill wall interactions, are depicted in Fig. 3. In this case, the column shear demands were estimated following the method described in Section 2 (see the calculation example in Supplementary Materials), and the maximum column shear demand to capacity ratios (V_d/V_c) of all buildings are listed in Table 1. The calculations were conducted in a story-by-story manner, following the proposed approach. These values were obtained from the critical direction corresponding to the y-axis of the building. The results show that all exterior columns in building B1 may have insufficient shear strength to resist the increased shear demand from the wall-frame interaction. The most critical columns were those located at the corners (C1) of the building. Insufficient shear strength was identified in the columns for all stories. Similarly, the exterior columns in the transverse and longitudinal directions (C2 and C3) also had insufficient strength, as shown in Table 1. For the interior columns (C4), sufficient column shear strength values were observed in all of the stories except for the 4th story. For building B2, insufficient shear strength values were observed only in the C1 columns for all stories and columns C2, C3, and C4 for the upper part of the building. It should be noted that building B2 was designed for higher seismic loads. As such, the columns exhibited a higher shear strength than those in building B1. The demand-to-capacity ratios of the columns in building B2 were mostly near or below one. Those with demand-to-capacity ratios greater than one were greater by only a small margin.

2.3 Performance evaluation of buildings without considering infill-frame interaction

Seismic performance assessments of the study buildings were performed using a 3-dimensional analytical model, as shown in Fig. 4. The model was implemented using the commercial structural analysis software SeismoStruct 2020 [46]. The building slab was assumed to be a rigid diaphragm, and full restraint was applied at the foundation level. The columns and beams were modeled using force-based fiber-section elements with five integration points. The well-known material constitutive

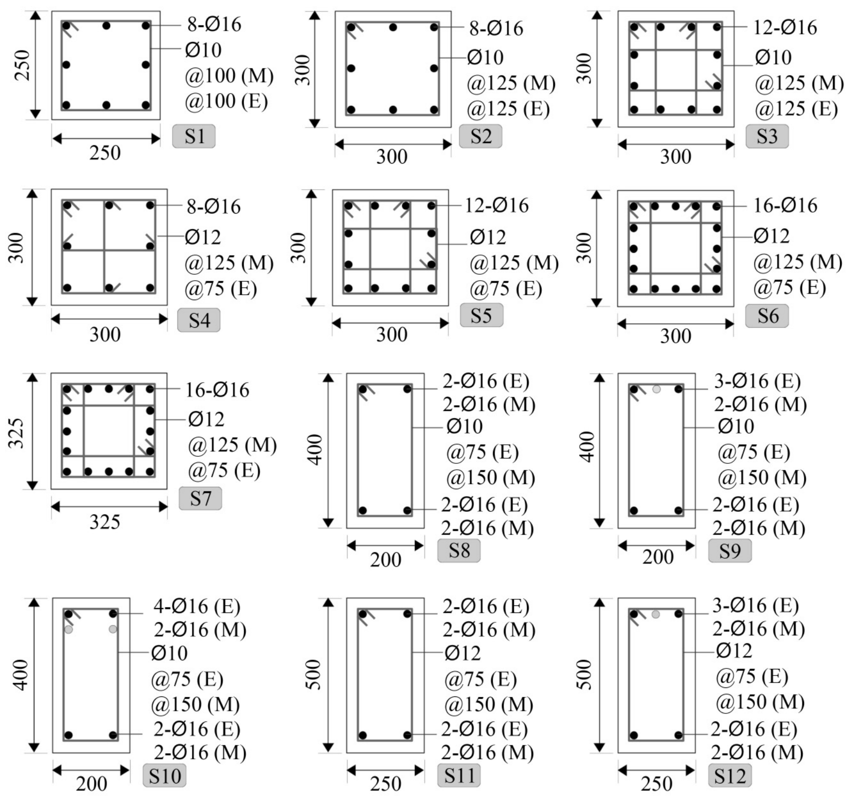

story	column				beam	
	C1	C2	C3	C4	Ext.	Int.
B1-building						
1st	S1	S1	S1	S3	S8	S9
2nd	S1	S1	S1	S2	S9	S10
3rd	S1	S1	S1	S1	S9	S10
4th	S1	S1	S1	S1	S9	S9
roof	-	-	-	-	S8	S8
B2-building						
1st	S4	S6	S6	S7	S11	S12
2nd	S4	S5	S5	S6	S12	S12
3rd	S4	S5	S5	S6	S12	S12
4th	S4	S4	S4	S6	S11	S12
roof	-	-	-	-	S11	S11

note:
All reinforcement are deformed bar, E is end zone, M is middle zone, Ext. is exterior, Int. is interior, and the unit is mm.

Fig. 3 Cross-section detail of columns and beams of buildings B1 and B2.

Table 1 Column shear demand to capacity ratios considering the infill-frame interaction

building	column	story			
		1st	2nd	3rd	4th
B1	C1	1.25	1.26	1.27	1.29
	C2	1.03	1.07	1.14	1.23
	C3	1.07	1.09	1.14	1.24
	C4	0.75	0.77	0.94	1.13
B2	C1	1.10	1.09	1.10	1.12
	C2	1.00	1.00	1.05	1.08
	C3	1.00	1.00	1.05	1.09
	C4	0.75	0.84	0.95	1.10

models, the Mander and Giuffre–Menegotto–Pinto models, were used for the concrete and reinforcement bars, respectively. It should be noted that the shear failure of RC members was not explicitly considered in the model to prevent numerical instability. The shear demand from the analysis was post-checked with the shear capacity to indicate shear failure. A simplified macro model using the equivalent compression strut concept was used for the masonry infill wall. To consider the local effect on the columns due to infill wall interaction, the infill walls were modeled using the multistrut model [11,29–31,47–49]. The compression-only 2-strut model proposed by Crisafulli and Carr [29] was adopted. The struts were oriented with one end located at the corner

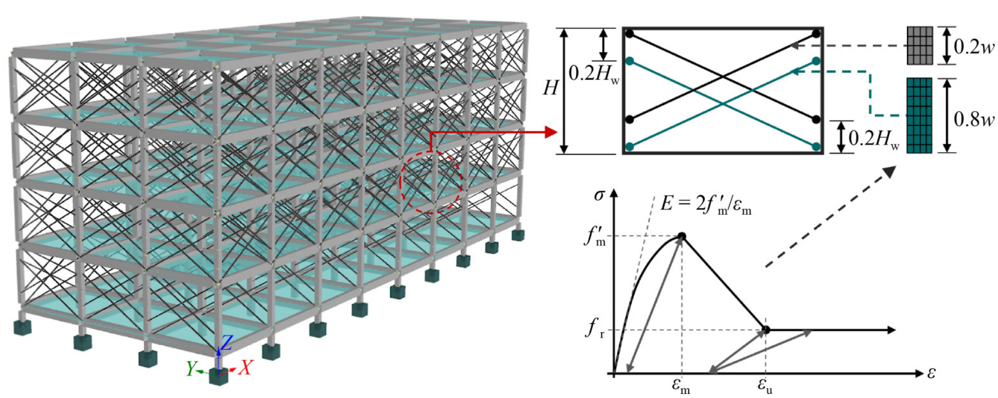

Fig. 4 Analytical model of the study buildings.

and the other at a distance of $0.2H_w$ from the top or bottom face of the beam (H_w is the infill wall height, as illustrated in Fig. 4). di Trapani et al. [49] indicated that struts can be modeled using fiber-section truss elements. A uniaxial material with the Kent−Scott−Park constitutive model was used. Calibration values of 0.0025 and 0.0060 were adopted for strains at the peak stress (ε_m) and at the residual point (ε_u), respectively. The residual strength (f_r) was assumed to be 0.1 times the masonry compressive strength (f'_m). According to the study reported by Wararuksajja et al. [36], the column shear demand strongly depends on the strength of the damaged infill strut, with the strength in the range 0.4–1.0 times the undamaged strength, depending on the structural response levels. When the infill wall damage zone extended to approximately $0.2H_w$, the reduction factor (α) was approximately equal to 0.8. Based on this observation, the strut width was assumed to be equal to $0.8w$ and $0.2w$ for the lower and upper struts, respectively, where w is the effective width of the total strut estimated by the formula proposed by Tucker [39]. This formula was evaluated based on an extensive literature review. To simplify the calculation, all the possible failure modes of the infill wall were combined into a single equation. In this method, the effective width of the equivalent strut is given by:

$$w = 0.25d_w(\lambda H)^{-1.15}, \tag{6}$$

where d_w is the diagonal length of the infill, H is the height of the frame, and λ is the relative stiffness of the surrounding frame and masonry infill wall proposed by Smith [3], which is given by:

$$\lambda = \sqrt[4]{\frac{E_m t_w \sin(2\theta)}{4EIH_w}}. \tag{7}$$

The initial strut strength of the solid infill wall was calculated as:

$$C_i = \psi f'_m w t_w. \tag{8}$$

In the above equations, E_m and E are the moduli of elasticity of the infill wall and concrete, respectively, t_w is the wall thickness, I is the moment of inertia of the column, and ψ is a numerical factor depending on the masonry type. In the present study, a value of 1.90 is specified for ψ. For an infill wall with an opening, the strut strength is reduced by applying the reduction factor to Eq. (8). The reduction factor of 0.4 was estimated through a finite element analysis of the one-bay, one-story, and infilled frames.

To investigate the capability of the proposed analytical model, single-bay and single-story bare and infilled RC frames as tested by Wararuksajja et al. [19,50], respectively, were used as references for model calibration. The specimens consisted of 0.30 m × 0.30 m columns, 3.0 m in height, a beam of 0.40 m × 0.20 m, and a length of 4.0 m. The infill wall was constructed with concrete blocks and plastered with strong mortar on both faces. The total thickness of the wall was approximately 0.10 m. Further information can be found in Wararuksajja et al. [19]. Analytical models of the infilled frames, as described previously, and the parameters shown in Table 2 were used to analyze the response of the frames.

3 Results and discussion

A comparison of the force−displacement hysteretic loops of the test specimen obtained by the analysis and experiment is shown in Fig. 5. For the bare RC frame, the analytical results match well with the experimental results. The peak lateral load of the specimen obtained analytically is within approximately 4% of that obtained experimentally. Both the analysis and the experiment

Table 2 Calibrated parameters used in the model

material	parameter	value
infill struts	w (mm)	255
	t_w (mm)	100
	$\psi f'_m$ (MPa)	14.63
	f_r (MPa)	1.46
	ε_m	0.0025
	ε_u	0.0060
concrete	E (GPa)	20.75
	f'_c (MPa)	19.50
	f'_t (MPa)	0.00
	ε_{cm}	0.003
reinforcement bar	E_s (GPa)	200
	f_y (MPa)	579
	S_t	0.02
	R_0	18.00
	R_1	0.97
	R_2	0.20
	A_1	0.10
	A_2	6.00
	A_3	0.10
	A_4	6.00
	f_i (MPa)	0.00
	ε_f	0.20

Note: f'_t is the tensile strength; ε_{cm} is the strain at peak compressive strength; E_s is the modulus of elasticity; S_t is the strain hardening parameter; R_0, R_1, and R_2 are the curvature parameters; A_1, A_2, A_3, and A_4 are the isotropic hardening parameters; f_i is the initial stress; ε_f is the fracture or buckling strain.

indicate that the failure mechanism of the specimen is formed by plastic hinges at the ends of the columns. For the infilled RC frame, the proposed model agrees reasonably well with the experimental results. The analytical results indicate that the peak lateral load resistance and stiffness of the specimen in the negative loading direction conforms to the experimental response. However, a larger difference is observed in the positive loading direction. The peak lateral load obtained from the analysis is approximately 10% less than that obtained experimentally. A small difference in the specimen drift at the peak resistance is also observed. The failure mechanisms of the infilled RC frame obtained from the analysis and experiment are compared in Fig. 6. Column shear failure and infill wall crushing are detected using the proposed model, as shown in Fig. 6(a). This failure mechanism matches well with the experimental observations (Fig. 6(b)). However, differences between the analysis and experiment are observed in terms of the drift. The analytical results indicate that the strength degradation of the infill wall (struts) initiated at approximately 0.75% drift, whereas it is observed in the experiment at approximately 0.5% drift. A similar difference can be observed for the drift at column shear failure. The analysis shows that the column shear starts at approximately 0.60% drift, whereas in the experiment, the shear crack became visible only at approximately 1.50% drift. This is expected because the simplified model is used to model the infill wall. Nevertheless, the proposed model is still acceptable for practical building performance assessments, as the results in terms of peak strength and drift at column shear failure are still conservative.

3.1 Nonlinear static analysis

Nonlinear pushover analyses were performed to gain further insight into the response. The main objective was to investigate the column failure mechanism of the studied buildings, especially when the building was

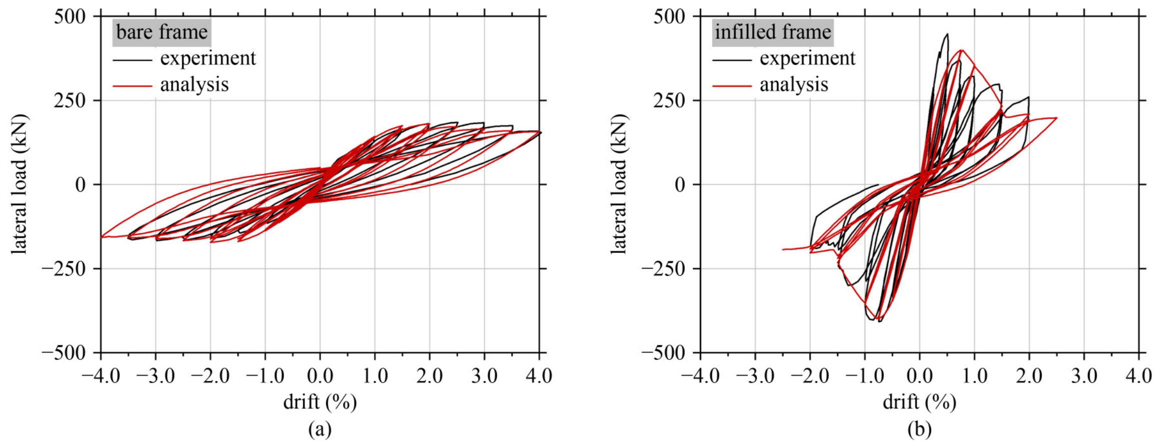

Fig. 5 Force−displacement comparison of the reference specimens. (a) Bare frame; (b) infillied frame.

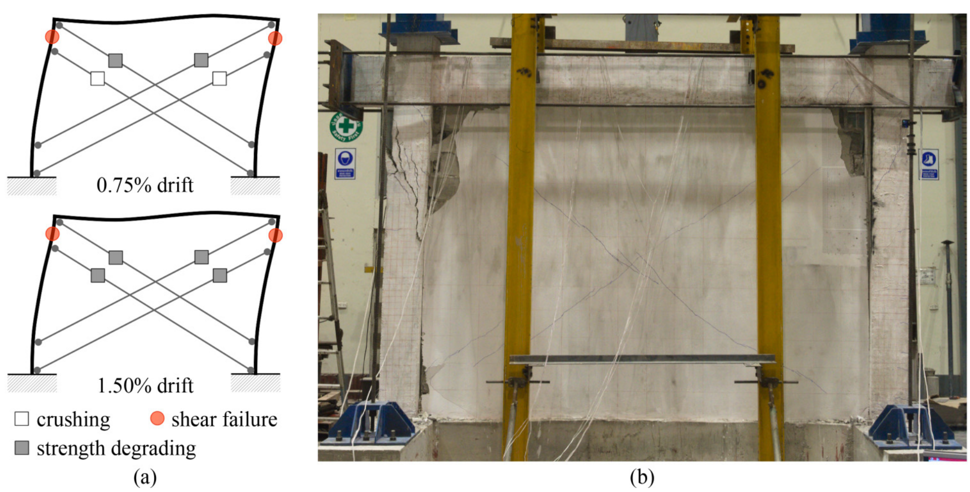

Fig. 6 Infilled frame failure mechanism obtained from: (a) analysis; (b) experiment [19]. (Reprinted from Bulletin of Earthquake Engineering, 18(14), Wararuksajja W, Srechai J, Leelataviwat S, Seismic design of RC moment-resisting frames with concrete block infill walls considering local infill-frame interactions, 6445–6474, Copyright 2020, with permission from Springer Nature.)

excited by ground motions stronger than those considered in the design process. Based on the observations described previously, the column shear failures were likely due to the response in the y-direction of the building. Therefore, only the results in this direction are provided. A conventional pushover with a specified lateral load pattern was used. As reported by ASCE/SEI 41-17 [35], multiple load patterns slightly improved the accuracy of the pushover analysis. ASCE/SEI 41-17 recommends the use of a single load pattern based on the shape of the first mode. Therefore, a lateral loading consistent with the first vibration mode was used in the present study. It should be noted that this procedure does not account for load pattern variation and higher mode effects. Therefore, it was suitable for low-rise and regular buildings, in which the first mode dominated their response. In other cases, the load pattern variation due to stiffness degradation and the higher mode effect are significant. For this reason, advanced procedures, such as modal pushover, adaptive pushover, and multimode pushover analyses should be considered. Extensive information and discussions on this topic can be found elsewhere [51–54].

Figure 7 shows the pushover curve and story drift of building B1. This building reached a peak resistance of 6498 kN at a roof drift of 0.40%. After this point, the load suddenly dropped owing to infill strut damage, and the 1st story drift increased rapidly as a result. The story drift profiles at different response levels are shown in Fig. 7(b). As expected, the infill strut forces induced columns shear failure in the 1st story of building B1, as shown in Fig. 8(a). Post-checks of the analysis results indicate that columns C1, C2, and C3 of the building will fail in shear. For the 1st story, this failure mechanism is consistent with the prediction using the design method discussed earlier. Nevertheless, column shear failures are not observed for the other stories.

The column shear demand-to-capacity ratios (V_d/V_c) of building B1 obtained by pushover analysis are plotted and compared with the values obtained by the proposed design method (predicted), as shown in Fig. 8(b). It

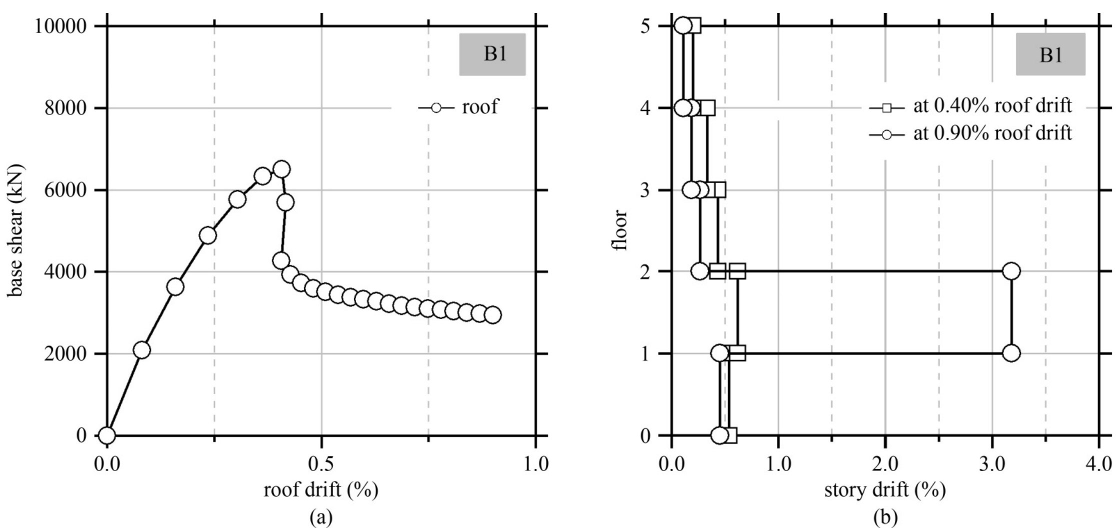

Fig. 7 Response of building B1: (a) pushover curve; (b) story drift.

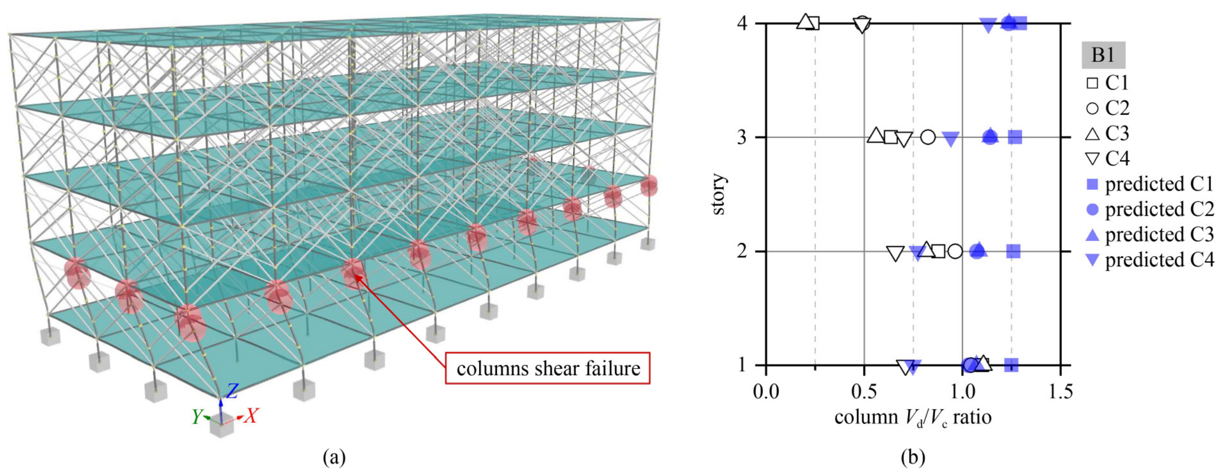

Fig. 8 Response of building B1: (a) failure mechanism; (b) column V_d/V_c ratios.

should be noted that the values plotted in the figure are the maximum enveloped for each column. Additionally, shear failure was not directly modeled, but was post-checked from the analysis results. Hence, the shear demand-to-capacity ratio is greater than one. In the pushover analysis, the maximum values occur for the 1st story and gradually decrease for the upper stories. For the 4th story, column V_d/V_c ratios ranging from 0.20 to 0.49 are observed. These observations differ considerably from those obtained using the proposed design method. However, the maximum V_d/V_c ratio occurs for the 4th story and gradually decreases for the lower stories. Hence, the largest difference in the column V_d/V_c ratios obtained by both methods occurs for the 4th story of the building.

Figure 9 shows the response of building B2. Overall, the response of this building is similar to that of building B1, showing a damage concentration for the 1st story. Figure 9(a) shows the pushover curves for building B2. This building reaches its peak resistance of 8557 kN at a roof drift of 0.38%. After this point, the load suddenly drops, and the first story drift increases rapidly as a result (Fig. 9(b)). The infill strut forces induce high column shear demand, particularly on the 1st story columns. However, the mechanism of building B2 is formed by flexural hinging of the columns without shear failure. This mechanism is slightly different from that predicted by using the column design method discussed earlier, in which the C1 columns of the building would fail in shear.

Figure 9(c) shows the column shear demand to capacity ratios (V_d/V_c) for building B2 obtained by pushover analysis compared with those obtained prior to the analysis using the proposed column design method. The column V_d/V_c ratio pattern is similar to that of building B1. The maximum values for all columns occurs in the 1st story and gradually decreases in the upper stories. For the 4th story, the column V_d/V_c ratios do not exceed 0.50. These values are significantly lower than those obtained by the proposed design method. Based on the pushover analysis, the column design method provides a reasonably accurate prediction of the column shear demand for the 1st and 2nd stories of the buildings. Overestimation is indicated for the upper part of the building, particularly for the top story. The inconsistency can be attributed to the exclusion of building global response in the estimation process. Therefore, the frame flexural capacity and the infill strut force are used without consideration for the story drift. This effect is explored in more detail in the subsequent sections. Given that the design method is based on an isolated column without considering the complex frame behavior and interactions, the estimated V_d/V_c ratios are within the acceptable margin. The prediction also errs on the conservative side, with V_d/V_c ratios higher than those obtained from the analysis.

3.2 Nonlinear response history analysis

Nonlinear response history analysis (NLRHA) were used to investigate the performance of the studied buildings under earthquake activity. In the present study, Rayleigh damping with a specified damping ratio of 5% was used for the first and last modes of interest. Seven pairs of ground-motion records were selected for each seismicity level. These records were scaled such that their spectra matched the maximum considered earthquake (MCE) spectrum according to the Thai seismic design code [55,56], as illustrated in Fig. 10. Each pair of ground motions was applied horizontally. Vertical ground motion was ignored in the analysis.

Under the considered ground motions, the envelopes of the story drifts in both orthogonal directions of building B1 are depicted in Fig. 11. The results show that the maximum and average values of the 1st story drift in the longitudinal x-direction are 2.01% and 1.34%, respectively, whereas the corresponding values in the transverse y-direction are approximately 0.84% and 0.40%, respectively. The average story drift in the x-direction is considerably higher than that in the y-direction, due to the number of infill walls present in each direction, which differ significantly. Furthermore, the deformations in the x-direction are concentrated in the 1st and 2nd stories and result from the infill wall damage. However, column shear failure is not observed in this direction. In the y-direction, the deformations tend to be distributed over

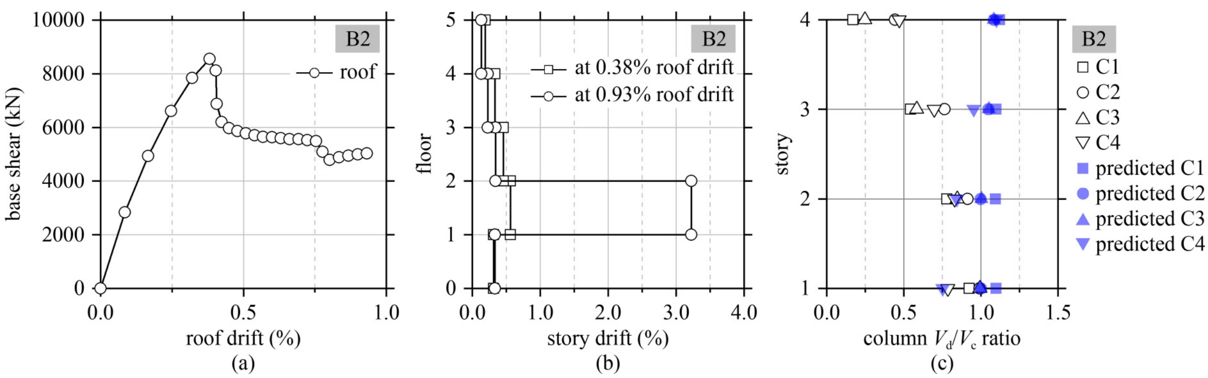

Fig. 9 Response of building B2: (a) pushover curve; (b) story drift; (c) column shear demand to capacity ratio.

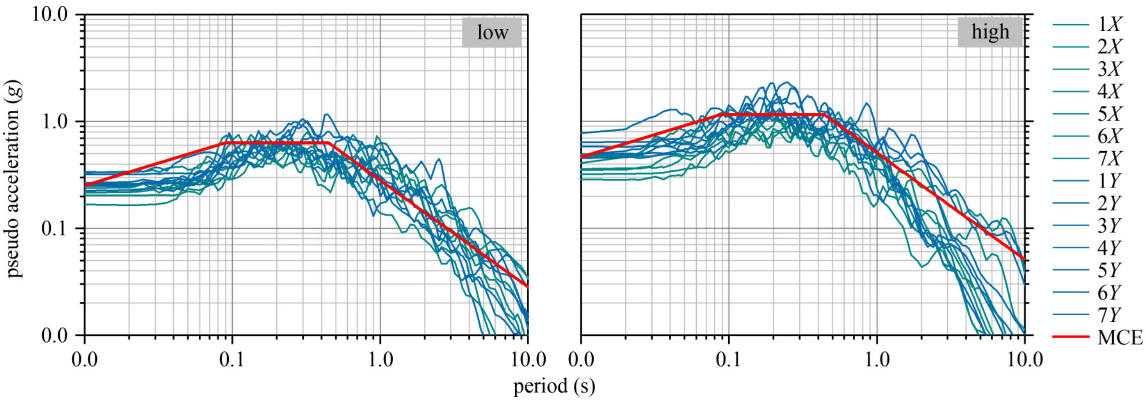

Fig. 10 Maximum considered earthquake spectrum and spectra of the selected ground motions.

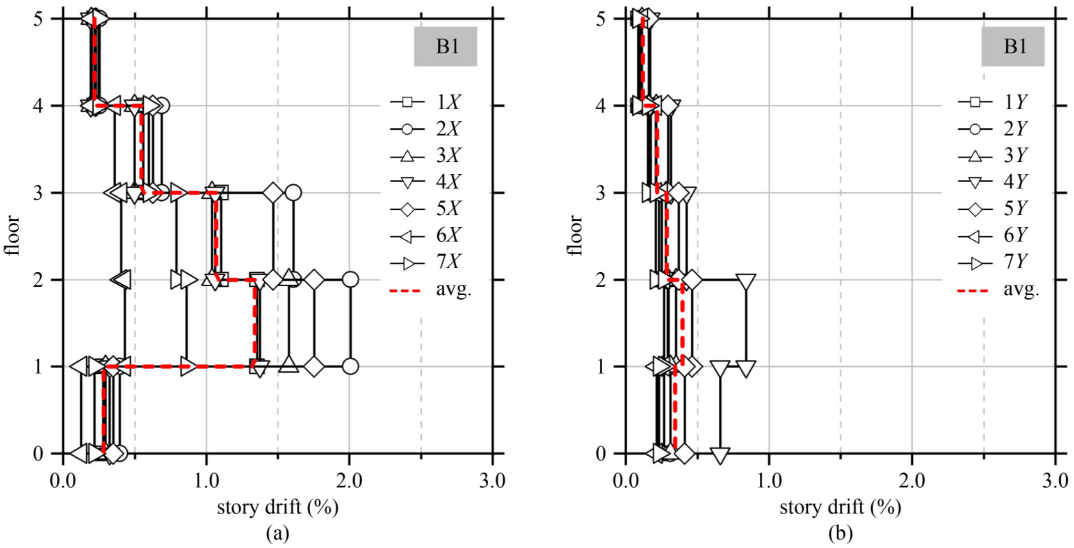

Fig. 11 Story drift envelopes of building B1 for the (a) longitudinal (x) and (b) transverse (y) directions.

the building height for all ground motions except ground motion No. 4. Under this ground motion, the infill struts on the 1st story of the building are damaged. As a result, the structural stiffness of this story significantly decreases, and the concentration of story drift occurs.

In terms of structural damage, the infill strut forces induce the shear failure of the columns in the 1st story, as indicated in Fig. 12. However, only the exterior columns (C1, C2, and C3) experience this failure. This failure mode is similar to that obtained from the pushover analysis. The V_d/V_c ratios of building B1 obtained by NLRHA are plotted in Fig. 13. It should be noted that the V_d/V_c ratios in the critical direction (y-direction) are also compared with the values obtained by the proposed design method (predicted). In the y-direction, maximum column V_d/V_c ratios of 0.92, 0.77, and 0.45 are observed for the 2nd, 3rd, and 4th stories, respectively. These values differ considerably from those obtained by the column design method, particularly for the top story of the building. For the corner and exterior columns (C1, C2, and C3), the V_d/V_c ratios are highest for the 1st story and decrease gradually over the building height. A different pattern of the column V_d/V_c ratio distribution is observed in the interior columns (C4). In this case, the maximum values occur in the 1st story and tend to remain constant until the 3rd story. The observed column V_d/V_c ratios in the x-direction are considerably lower than those in the y-direction. The maximum value of 0.48 is observed for column C4 in the 1st story of the building. In the x-direction, there are two types of columns: those bounded by the infill wall on the sides and those that are not in contact with the infill wall. For columns C1 and C3, which are connected to the infill wall, the maximum V_d/V_c ratios occur for the 1st story and tend to remain constant up to the 3rd story. As expected, a different column V_d/V_c ratio distribution pattern is observed for columns C2 and C4, which are not in contact with the infill wall. In this case, a linear distribution profile with the highest value in the first story is observed.

The envelopes of the story drifts in both orthogonal directions for building B2 are shown in Fig. 14. Overall, the responses of this building are comparable to those of building B1, although they exhibit considerably different story drift values in both directions. The maximum and

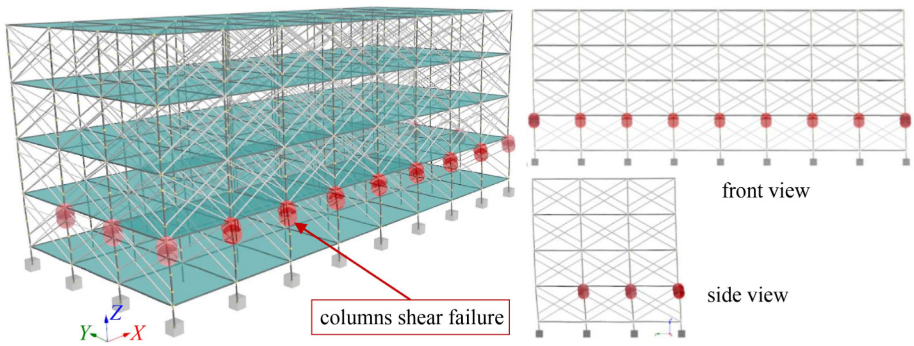

Fig. 12 Column shear failure of the B1 building.

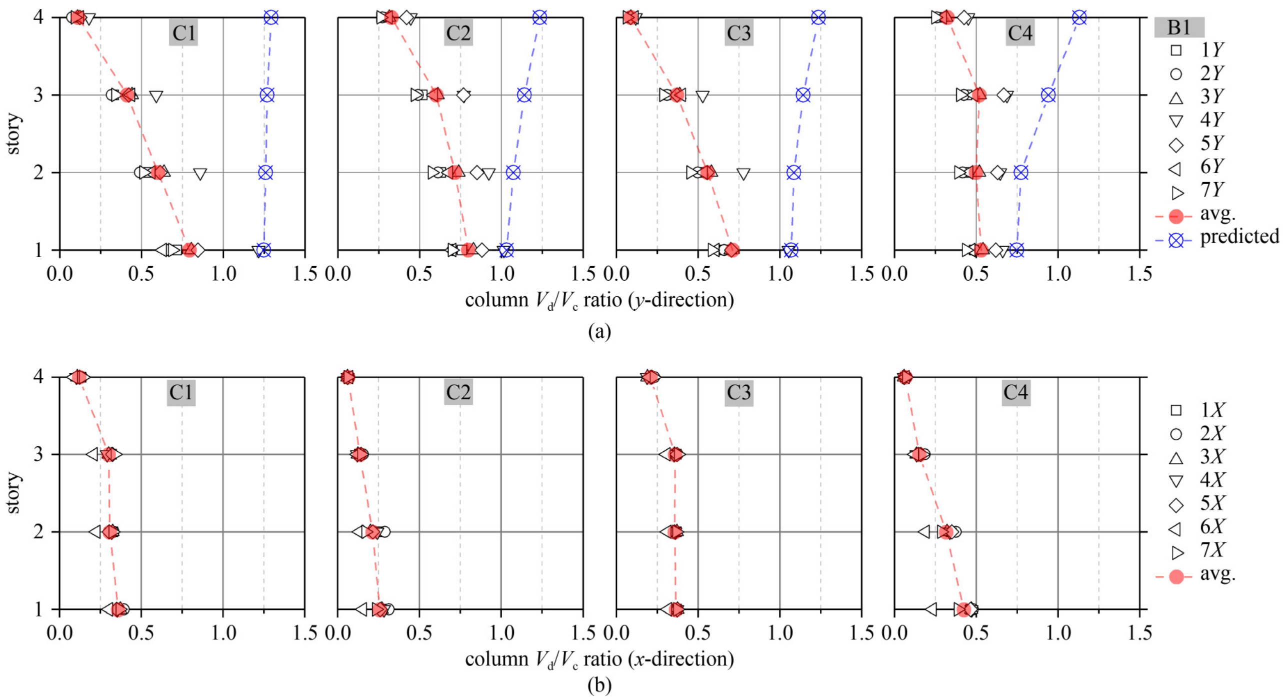

Fig. 13 Column shear demand to capacity ratio of building B1: (a) y-direction; (b) x-direction.

average values of the 1st story drift in the x-direction are 1.72% and 1.14%, respectively, whereas those in the y-direction are approximately 1.25% and 0.87%, respectively. In the x-direction, the deformations tend to be concentrated in the 1st and 2nd stories, possibly because of infill wall damage. The deformations in the y-direction tend to be distributed over the height of the building, whereas the damaged infill strut induces drift concentration for the 1st story. Flexural damage to the columns, including reinforcement yielding and concrete crushing, is also observed. However, column shear failure is not observed in either direction.

For building B2, there is a slight difference between the shear demand prediction and analysis results. According to the prediction, shear failure of C1 columns can be expected in these buildings. However, the NLRHA results indicate no shear failure in these columns. Figure 15 shows the column V_d/V_c ratios of building B2 obtained from the time history analyses. In the y-direction, maximum values of 0.98, 0.99, 0.99, and 0.88 are observed for columns C1, C2, C3, and C4, respectively. All these values occur in the 1st story of the building, except for the C4 columns, in which the maximum value is detected in the 3rd story. For columns C1, C2, and C3, the column V_d/V_c ratios obtained in the 1st story match the values obtained from the proposed design method (predicted) reasonably well. However, differences arise in the upper stories, particularly the top story. The column V_d/V_c ratios in the x-direction are considerably lower than those in the y-direction. The maximum value of 0.52 is measured on column C3 in the 1st story.

Overall, the NLRHA provides similar results to those obtained from the pushover analysis, which shows that the column design method is acceptable for predicting the column shear demand on the 1st and 2nd stories of the buildings. This method overestimates the shear demand for the upper part of the building, particularly in the top story. The main reason for this is that the simplified method does not consider the global building response in the estimation process. The column or beam plastic moment (M_p) and infill strut force (αC_i) are used without considering the building drift. This is consistent with the plastic mechanism of the isolated column. Figure 16 shows the distributions of the normalized maximum infill strut force, column shear demand, and story drift corresponding to the maximum strut force. In this figure, the maximum infill strut force and column shear demand that occur on each story are divided by the corresponding values obtained on the 1st story. For the normalized story drift, the drift when the infill strut force reaches the maximum value is selected for each story. These values are then divided by the corresponding values obtained in the 1st story. The results indicate that both the infill strut force and column shear demand depend strongly on the story drift of the building. In the y-direction, the infill strut force values in the 3rd and 4th stories never exceed 75% of the infill strut force in the 1st story. However, in the calculation, the same strut force is used in all stories. The overestimation of the infill strut forces lead to an overestimation of the column shear demand values. Although a more accurate result can be expected if the building story drift is considered in the estimation

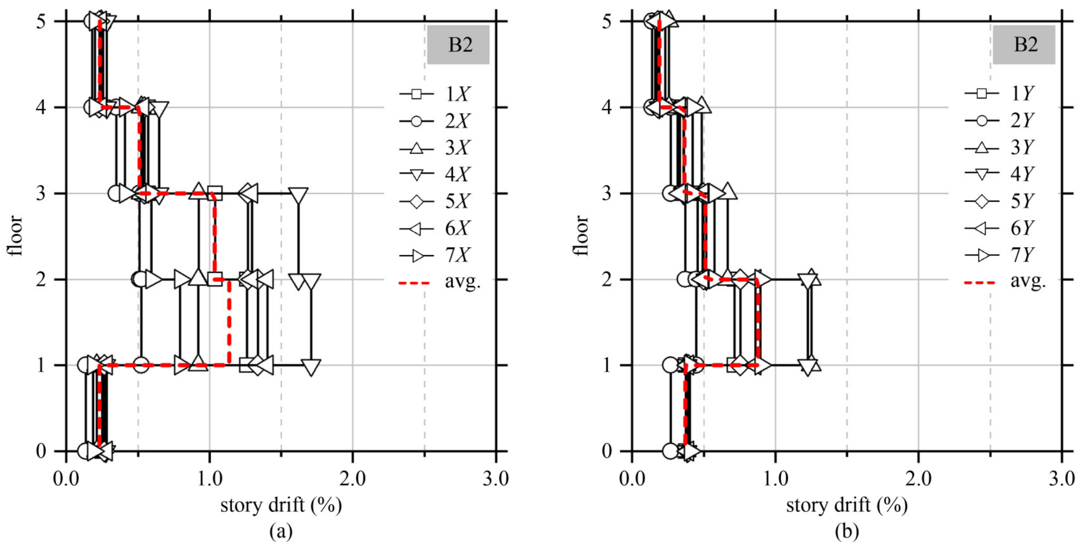

Fig. 14 Story drift envelopes of building B2 for the (a) longitudinal (x) and (b) transverse (y) directions.

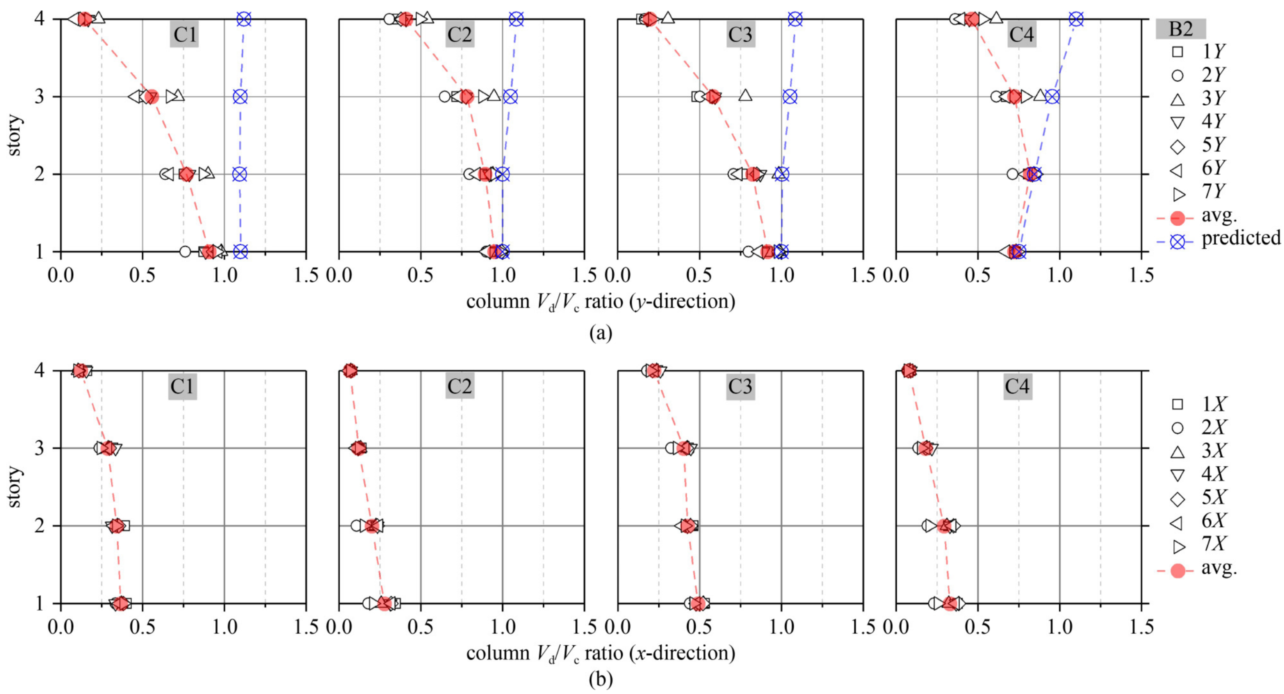

Fig. 15 Column shear demand to capacity ratio of building B2: (a) y-direction; (b) x-direction.

procedure, several parameters can affect the story drift profile of the building, making it impractical to use it as a design parameter.

3.3 Performance evaluation of buildings designed following the proposed strategies

To investigate the effectiveness of the design strategies presented in Section 2, the building was redesigned according to the presented procedure. According to the seismic performance assessment of the buildings described earlier, insufficient column shear strength was observed in building B1, both from the shear demand estimation using the proposed method and from the detailed nonlinear analysis. For building B2, the shear demand estimation appears to be slightly conservative, and a detailed nonlinear analysis indicates that the columns have sufficient shear strength. Therefore, the redesign process considering the infill-frame interaction was conducted only on building B1. The redesigned building was denoted as building B1R. It should be noted that the design method described in Section 2 was applied to the columns for all stories of the building. However, in reality, the high column shear demands are concentrated only on the first few stories. The redesigned column cross section and reinforcement details are shown in Fig. 17. The other details were the same. After the redesign process, the performance of the redesigned building B1R was reassessed using pushover analysis and NLRHA. The key results are as follows.

The overall responses of building B1R are similar to those of building B1, with a slightly higher peak resistance and different story drift values, as depicted in Fig. 18. However, a key difference arises in terms of column failure, where no column shear failure is detected in the redesigned building. The column V_d/V_c ratios for both cases are plotted and compared in Fig. 19. As shown in this figure, the column V_d/V_c ratio distribution profiles of these buildings are comparable. For the building B1R, the maximum value of 0.84 is found for C2 columns. As expected, high column V_d/V_c ratios occur only in the 1st and 2nd stories of the building.

For the NLRHA results, the overall response of building B1R is similar to that of building B1, as described previously. The envelopes of the story drifts in both orthogonal directions of the building B1R under the considered ground motions are depicted in Fig. 20. The results show that the maximum and average values of the first-story drift in the *x*-direction are 1.94% and 1.29%, respectively, whereas the corresponding values in the *y*-direction are approximately 0.94% and 0.40%, respectively. In addition, the average envelopes of the story drift in the *x*- and *y*-direction of buildings B1 and B1R are compared. Some differences in the story drift values are observed in the *x*-direction owing to the variation in the column stiffness. Unlike building B1, column shear failure is not observed in building B1R. The column shear demand-to-capacity ratios (V_d/V_c) in the critical direction (*y*-direction) are shown in Fig. 21. The maximum values of 0.75, 0.84, 0.81, and 0.66 are found for columns C1, C2, C3, and C4, respectively. For columns C1 and C3, the predicted V_d/V_c ratios for the 1st

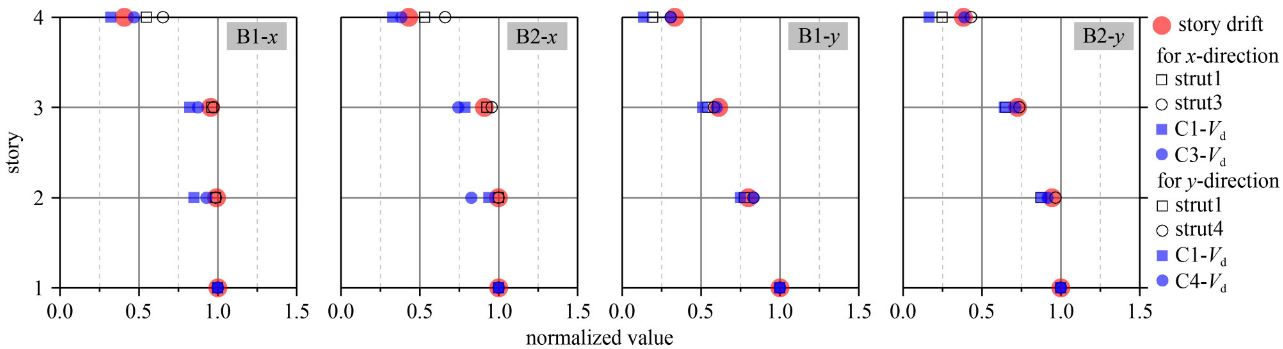

Fig. 16 Normalization of strut force, column shear demand, and story drift.

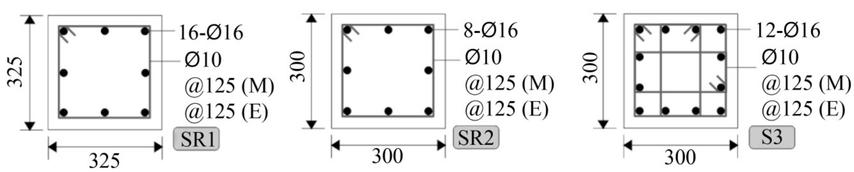

Note:
All reinforcement are deformed bar, E is end zone, M is middle zone, and the unit is mm.

story	column			
	C1	C2	C3	C4
B1R-building				
1st	SR1	SR2	SR2	S3
2nd	SR1	SR2	SR2	SR2
3rd	SR1	SR2	SR2	SR2
4th	SR1	SR2	SR2	SR2

Fig. 17 Cross-section details of the redesigned columns of the redesigned building B1R.

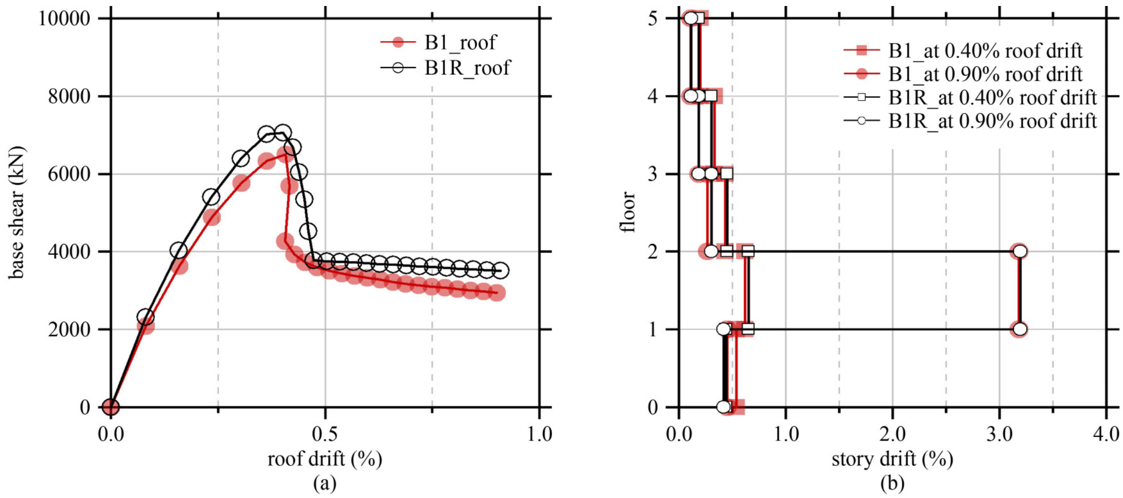

Fig. 18 Response of buildings B1 and B1R: (a) pushover curve; (b) story drift.

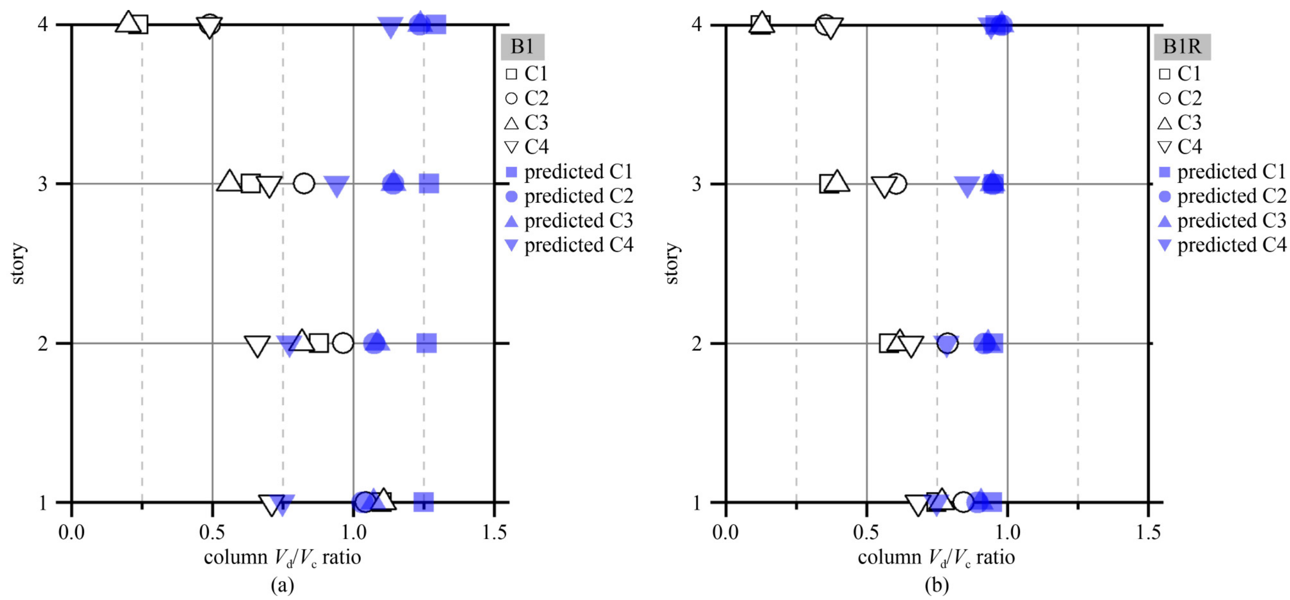

Fig. 19 Column shear demand to capacity ratio of buildings: (a) B1 and (b) B1R.

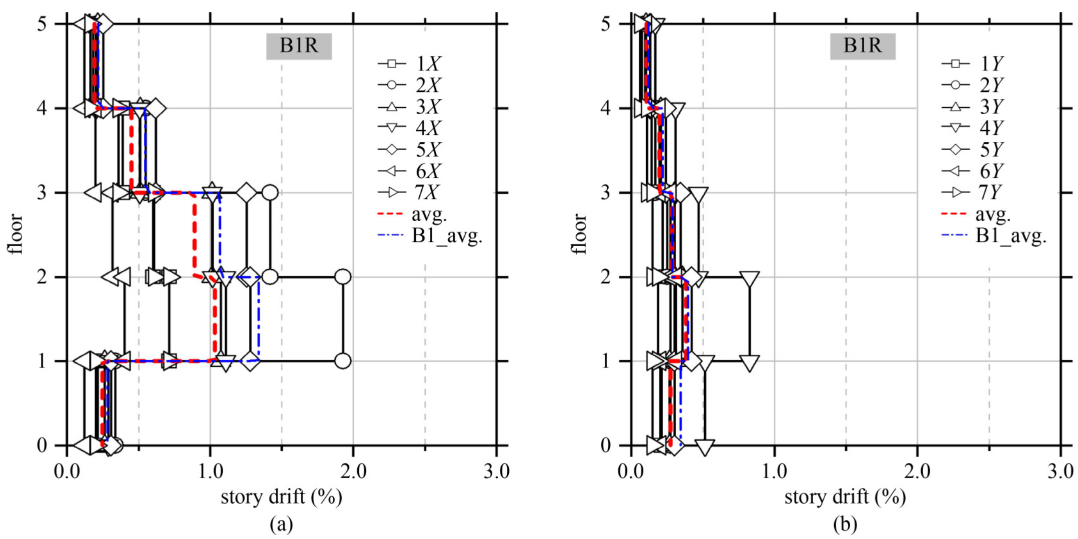

Fig. 20 Inter-story drift envelopes of the building B1R for the (a) longitudinal (x) and (b) transverse (y) direction.

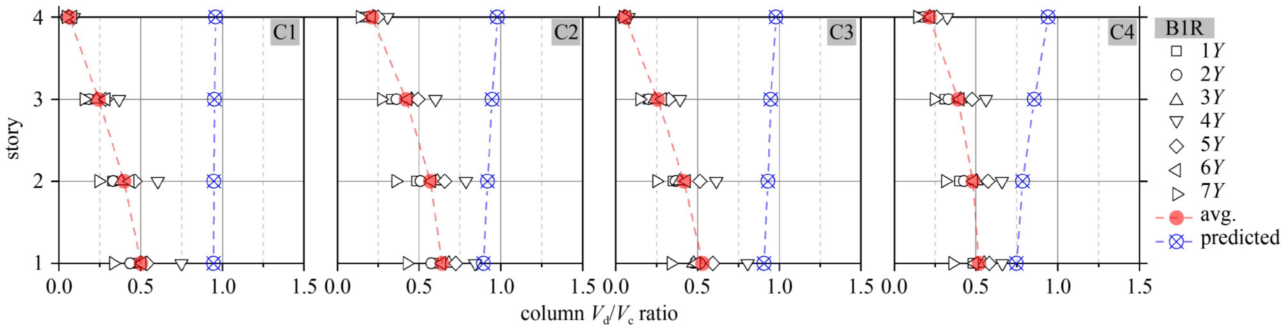

Fig. 21 Column shear demand to capacity ratio of the building B1R.

story of the building are reasonably accurate.

According to the results presented, the column design method that considers the infill wall-frame interaction can eliminate column shear failure. Without considering the building's global response, the method overestimates the column shear demand, particularly in the upper part of the building. Nevertheless, from a design perspective, this method is useful and practical for preventing undesirable failure modes in columns.

4 Conclusions

In this study, an effective design strategy that considers infill-frame interactions was investigated. The main concept of the design approach is briefly reviewed. Two RC buildings with infill walls, located in areas with different seismicity levels in Thailand, were used as examples. Two design cases were considered: one with and one without consideration for the local interaction of the infill walls, following the proposed design method. The performance of these buildings was assessed using nonlinear static and dynamic analyses. The failure modes, key responses of the studied buildings, and effectiveness of the proposed design approach are also discussed.

Based on the study results, the overall responses of the buildings designed with and without consideration for the local interaction of the infill walls are similar. Only minor differences of approximately 8% are observed in the peak load resistance. Although the overall lateral strengths are relatively similar, column shear failure occurs in the designed building without consideration for the infill walls but not in the counterpart building. The local shear failures of the first-story columns predicted by the proposed method are in good agreement with the analytical results. More importantly, by applying this design method, column shear failure can be eliminated. However, the method still overestimates the column shear demand, particularly in the upper part of the building. The results show that the shear demand in the upper part of the building, particularly at the top level, can be overestimated by approximately eight times and three times for the exterior and interior columns, respectively. This limitation is primarily because the plastic mechanism analysis ignores the actual story drift response of the building in the design method. The results show that only the first story is critical, whereas the upper part of the study buildings respond primarily in the elastic stage. The design can be improved if the variation in the story drift is considered. Thus, the story drift profile of the building is found to be the key to improving the accuracy of the method. However, to obtain the necessary information, nonlinear analysis of the infilled frame must be conducted. If necessary, these nonlinear analysis results may be used in design iterations or as a final design check. Although further investigations are required before the proposed method can be fully validated, the study demonstrates the potential of this practical approach. Additionally, the accuracy of the design method strongly depends on the infill strut capacity. A large variation in the infill wall strength may exist depending on several factors, especially the local material characteristics and construction practices. Therefore, the infill strut capacity should be estimated using an appropriate approach calibrated with locally available materials.

Acknowledgements The authors gratefully acknowledge the financial support from the Thailand Research and Innovation under Fundamental Fund 2022 (Advanced Construction Toward Thailand 4.0 Project) to the Construction Innovations and Future Infrastructures Research Center at King Mongkut's University of Technology Thonburi. Supplementary funding was provided by TRF Senior Research Scholar under Grant RTA 6280012.

Electronic Supplementary Material Supplementary material is available in the online version of this article at https://doi.org/10.1007/s11709-023-0937-2 and is accessible for authorized users.

References

1. Sezen H, Whittaker A S, Elwood K J, Mosalam K M. Performance of reinforced concrete buildings during the August 17, 1999 Kocaeli, Turkey earthquake, and seismic design and construction practise in Turkey. Engineering Structures, 2003, 25(1): 103−114
2. Ferraioli M, Lavino A. Irregularity effects of masonry infills on nonlinear seismic behaviour of RC buildings. Mathematical

Problems in Engineering, 2020, 2020: 4086320
3. Smith B S. Lateral stiffness of infilled frames. Journal of the Structural Division, 1962, 88(6): 183−199
4. Paulay T, Priestly M J N. Seismic Design of Reinforced Concrete and Masonry Buildings. New York: Wiley, 1992
5. Saneinejad A, Hobbs B. Inelastic design of infilled frames. Journal of Structural Engineering, 1995, 121(4): 634−650
6. Fardis M N, Panagiotakos T B. Seismic design and response of bare and masonry-infilled reinforced concrete buildings. Part II: Infilled structures. Journal of Earthquake Engineering, 1997, 1(3): 475−503
7. Asteris P G. Lateral stiffness of brick masonry infilled plane frames. Journal of Structural Engineering, 2003, 129(8): 1071−1079
8. Bertero V, Brokken S. Infills in seismic resistant building. Journal of Structural Engineering, 1983, 109(6): 1337−1361
9. Blasi G, Perrone D, Aiello M A. Fragility functions and floor spectra of RC masonry infilled frames: Influence of mechanical properties of masonry infills. Bulletin of Earthquake Engineering, 2018, 16(12): 6105−6130
10. Asteris P G, Repapis C C, Cavaleri L, Sarhosis V, Athanasopoulou A. On the fundamental period of infilled RC frame buildings. Structural Engineering and Mechanics, 2015, 54(6): 1175−1200
11. Burton H, Deierlein G. Simulation of seismic collapse in nonductile reinforced concrete frame buildings with masonry infills. Journal of Structural Engineering, 2014, 140(8): A4014016
12. Mehrabi A B, Shing P B, Schuller M P, Noland J L. Experimental evaluation of masonry-infilled RC frames. Journal of Structural Engineering, 1996, 122(3): 228−237
13. Al-Chaar G, Issa M, Sweeney S. Behavior of masonry-infilled nonductile reinforced concrete frames. Journal of Structural Engineering, 2002, 128(8): 1055−1063
14. Srechai J, Lukkunaprasit P. An innovative scheme for retrofitting masonry-infilled non-ductile reinforced concrete frames. The IES Journal Part A: Civil & Structural Engineering, 2013, 6(4): 277−289
15. Niyompanitpattana S, Warnitchai P. Effects of masonry infill walls with openings on seismic behaviour of long-span GLD RC frames. Magazine of Concrete Research, 2017, 69(21): 1082−1102
16. Su Q, Cai G, Cai H. Seismic behaviour of full-scale hollow bricks-infilled RC frames under cyclic loads. Bulletin of Earthquake Engineering, 2017, 15(7): 2981−3012
17. Suzuki T, Choi H, Sanada Y, Nakano Y, Matsukawa K, Paul D, Gülkan P, Binici B. Experimental evaluation of the in-plane behaviour of masonry wall infilled RC frames. Bulletin of Earthquake Engineering, 2017, 15(10): 4245−4267
18. Alwashali H, Sen D, Jin K, Maeda M. Experimental investigation of influences of several parameters on seismic capacity of masonry infilled reinforced concrete frame. Engineering Structures, 2019, 189: 11−24
19. Wararuksajja W, Srechai J, Leelataviwat S. Seismic design of RC moment-resisting frames with concrete block infill walls considering local infill-frame interactions. Bulletin of Earthquake Engineering, 2020, 18(14): 6445−6474
20. Stavridis A, Shing P B. Finite-element modeling of nonlinear behavior of masonry-infilled RC frames. Journal of Structural Engineering, 2010, 136(3): 285−296
21. Koutromanos I, Stavridis A, Shing P B, Willam K. Numerical modeling of masonry-infilled RC frames subjected to seismic loads. Computers & Structures, 2011, 89(11−12): 1026−1037
22. Milanesi R R, Morandi P, Magenes G. Local effects on RC frames induced by AAC masonry infills through FEM simulation of in-plane tests. Bulletin of Earthquake Engineering, 2018, 16(9): 4053−4080
23. Cavaleri L, Di Trapani F. Prediction of the additional shear action on frame members due to infills. Bulletin of Earthquake Engineering, 2015, 13(5): 1425−1454
24. Srechai J, Leelataviwat S, Wongkaew A, Lukkunaprasit P. Experimental and analytical evaluation of a low-cost seismic retrofitting method for masonry-infilled non-ductile RC frames. Earthquakes and Structures, 2017, 12(6): 699−712
25. Basha S H, Kaushik H B. A novel macromodel for prediction of shear failure in columns of masonry infilled RC frames under earthquake loading. Bulletin of Earthquake Engineering, 2019, 17(4): 2219−2244
26. Huang H, Burton H V. A database of test results from steel and reinforced concrete infilled frame experiments. Earthquake Spectra, 2020, 36(3): 1525−1548
27. Kaushik H B, Rai D C, Jain S K. Code approaches to seismic design of masonry-infilled reinforced concrete frames: A state-of-the-art review. Earthquake Spectra, 2006, 22(4): 961−983
28. El-Dakhakhni W W, Elgaaly M, Hamid A A. Three-strut model for concrete masonry-infilled steel frames. Journal of Structural Engineering, 2003, 129(2): 177−185
29. Crisafulli F J, Carr A J. Proposed macro-model for the analysis of infilled frame structures. Bulletin of the New Zealand Society for Earthquake Engineering, 2007, 40(2): 69−77
30. Asteris P G, Antoniou S T, Sophianopoulos D S, Chrysostomou C Z. Mathematical macromodeling of infilled frames: State of the art. Journal of Structural Engineering, 2011, 137(12): 1508−1517
31. Nicola T, Leandro C, Guido C, Enrico S. Masonry infilled frame structures: State-of-the-art review of numerical modelling. Earthquakes and Structures, 2015, 8(1): 225−251
32. Srechai J, Leelataviwat S, Wararuksajja W, Limkatanyu S. Multi-strut and empirical formula-based macro modeling for masonry infilled RC frames. Engineering Structures, 2022, 266: 114559
33. Dhir P K, Tubaldi E, Ahmadi H, Gough J. Numerical modelling of reinforced concrete frames with masonry infills and rubber joints. Engineering Structures, 2021, 246: 112833
34. European Committee for Standardization (CEN). Design of Structures for Earthquake Resistance—Part 1: General Rules, Seismic Actions and Rules for Buildings, EN 1998-1, Eurocode 8. Brussels: European Committee for Standardization, 2004
35. American Society of Civil Engineers (ASCE). Seismic Evaluation and Retrofit of Existing Buildings, ASCE/SEI 41-17. Reston, VA: ASCE, 2017
36. Wararuksajja W, Srechai J, Leelataviwat S, Sungkamongkol T, Limkatanyu S. Seismic design method for preventing column shear failure in reinforced concrete frames with infill walls. Journal of Building Engineering, 2021, 44: 102963
37. Smith B S, Coull A. Tall Building Structures: Analysis and Design. New York: Wiley, 1991

38. Federal Emergency Management Agency (FEMA). Evaluation of Earthquake Damaged Concrete and Masonry Wall Buildings: Basic Procedures Manual, FEMA 306. Washington, D.C.: FEMA, 1999
39. Tucker C J. Prediction the in-plane capacity of masonry infilled frames, in Faculty of the Graduate School. Dissertation for the Doctoral Degree. Cookeville, TN: Tennessee Technological University, 2007, 270
40. Stavridis A. Analytical and Experimental Study of Seismic Performance of Reinforced Concrete Frames Infilled with Masonry Walls. La Jolla, CA: University of California San Diego, 2009, 417
41. Masonry Standard Joint Committee (MSJC). Building Code Requirements and Specification for Masonry Structures, TMS 402-11. Longmont, CO: MSJC, 2011
42. Moretti M, Tassios T. Behaviour of short columns subjected to cyclic shear displacements: Experimental results. Engineering Structures, 2007, 29(8): 2018−2029
43. Li Y A, Hwang S J. Shear behavior prediction of non-ductile reinforced concrete members in earthquake. In: Hsu T T C, ed. Concrete Structures in Earthquake. Singapore: Springer Singapore, 2019, 17–27
44. Li Y A, Hwang S J. Prediction of lateral load displacement curves for reinforced concrete short columns failed in shear. Journal of Structural Engineering, 2017, 143(2): 04016164
45. American Concrete Institute (ACI). Building Code Requirements for Structural Concrete and Commentary, ACI 318/318R-14. Farmington Hills, MI: ACI, 2014
46. SeismoStruct: Civil engineering software for structural assessment and structural retrofitting. Pavia: SeismoSoft–Earthquake Engineering Software Solutions. 2020
47. Sattar S, Liel A B. Seismic performance of nonductile reinforced concrete frames with masonry infill walls—I: Development of a strut model enhanced by finite element models. Earthquake Spectra, 2016, 32(2): 795−818
48. Mohammad Noh N, Liberatore L, Mollaioli F, Tesfamariam S. Modelling of masonry infilled RC frames subjected to cyclic loads: State of the art review and modelling with OpenSees. Engineering Structures, 2017, 150: 599−621
49. di Trapani F, Bertagnoli G, Ferrotto M F, Gino D. Empirical equations for the direct definition of stress−strain laws for fiber-section-based macromodeling of infilled frames. Journal of Engineering Mechanics, 2018, 144(11): 04018101
50. Wararuksajja W. Seismic behavior and design of reinforced concrete moment resisting frames with concrete block infill walls considering infill-frame interactions. Dissertation for the Doctoral Degree. Bangkok: King Mongkut's University of Technology Thonburi, 2020, 216
51. Chopra A K, Goel R K, Chintanapakdee C. Evaluation of a modified MPA procedure assuming higher modes as elastic to estimate seismic demands. Earthquake Spectra, 2004, 20(3): 757−778
52. Antoniou S, Pinho R. Advantages and limitations of adaptive and non-adaptive force-based pushover procedures. Journal of Earthquake Engineering, 2004, 8(4): 497−522
53. Ferraioli M, Lavino A, Mandara A. An adaptive capacity spectrum method for estimating seismic response of steel moment-resisting frames. Ingegneria Sismica, 2016, 1(2): 47−60
54. Ferraioli M. Multi-mode pushover procedure for deformation demand estimates of steel moment-resisting frames. International Journal of Steel Structures, 2017, 17(2): 653−676
55. Department of Public Works and Town & Country Planning (DPT). Companion Standard for Seismic Design of Building Structures in Thailand, DPT 1301-54. Bangkok: DPT, 2011 (in Thai)
56. Department of Public Works and Town & Country Planning (DPT). Standard for Seismic Design of Building Structures in Thailand, DPT 1301-52. Bangkok: DPT, 2009 (in Thai)